Phase Behavior of Methane–Ethane Mixtures in Nanopores

T. Pitakbunkate†, T. A. Blasingame†, G. J. Moridis†, and P. B. Balbuena*‡

†Department of Petroleum Engineering and ‡Department of Chemical Engineering, Texas A&M University, College Station, Texas 77843, United States

*E-mail: balbuena@tamu.edu.

Abstract

The behavior of fluids in confined spaces is important in several research fields, including the oil and gas industry, because of the importance of confined hydrocarbons in unconventional shale reservoirs. A large percentage of the hydrocarbons are contained in nanoscale shale pores, and as a result, interactions between fluid molecules and the pore walls become significant to the fluid behavior and cause deviations of the fluid properties from bulk properties. In this work, classical molecular dynamics (MD) simulations and grand canonical Monte Carlo (GCMC) simulations are performed to model kerogen pores in shale reservoirs and their effect on adsorption selectivity and phase equilibria of hydrocarbon mixtures in a wide range of temperatures and pressures. A slit pore made of graphite walls is used to represent the basic unit where a fluid may be stored in shale reservoirs. The separation between graphite layers is varied to observe the effect of confinement on the adsorption selectivity and phase equilibrium of methane–ethane mixtures. Results from GCMC and MD simulations show that ethane is preferred over methane in the confined system. Moreover, most fluid molecules in the confined system tend to be adsorbed on the pore walls instead of remaining in the gas phase. Preferential interactions between the fluid molecules and the pore walls induce changes in the phase diagram in the confined system. Results from GCMC simulations show shifts with respect to the bulk pressure–composition phase diagram that becomes more pronounced as the pore size decreases.

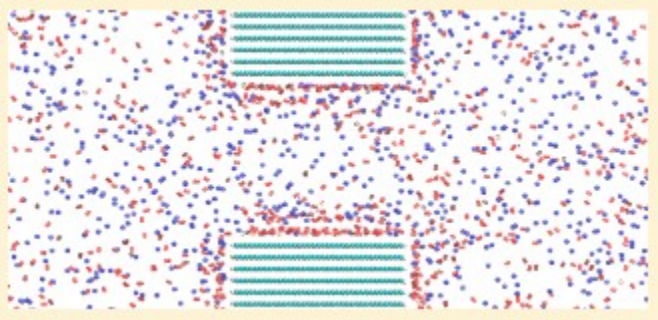

Introduction

On the basis of the 2015 U.S. Energy Information Administration (EIA) report, estimates of U.S. recoverable tight oil resources and wet shale gas resources are 78.2 billion barrels (#1 in ranking of 46 countries) and 622.5 trillion cubic feet (#4 in ranking of 46 countries), respectively. It implies that

unconventional oil and gas resources may play an important role in U.S. oil production. Shale is a fine-grained, clastic sedimentary rock. Its structure consists of a mix of flakes of clay minerals, as well as organic matter called kerogen and tiny fragments of other minerals, such as quartz and calcite. Hydrocarbons are stored in both the inorganic and organic pores of shale reservoirs. The organic pores are voids in the kerogen structure.(1-5) As a result, the study of confined hydrocarbon mixtures is crucial to help petroleum engineers understand the mechanism of hydrocarbon storage and flow in shale reservoirs. Hydrocarbons may be stored in shale reservoirs by various mechanisms: (1) adsorption on surfaces, (2) conventional storage in natural and hydraulic fractures, (3) conventional storage in pores of the matrix, (4) solution in formation water, and (5) adsorption in organic matter. (6) The current hydrocarbon recovery from shale reservoirs is usually 5% or less.(7)

Thus, a deeper understanding of the phase behavior of fluid systems in nanopores is needed to help enhancing hydrocarbon recovery from shale reservoirs. As a result, in the past decade, numerous studies have been performed to describe the storage and transport of hydrocarbons in shale reservoirs. The purpose of these studies is mainly to improve estimation and production forecasts of reserves. Desorption–adsorption models (e.g., Langmuir model) added to the numerical simulations and gas-in-place calculations are used to account for adsorbed gas in shales.(8-11) A phase envelope of a multicomponent confined mixture computed by a correlation and algorithm was proposed by Stenby et al. to capture the effect of capillary pressure in a confined space.(12) Knudsen diffusion and slip flow models are integrated in numerical simulations to capture a microflow regime that may occur in shale reservoirs.(8, 13-15) These studies were developed by modifying correlations used for conventional reservoirs. However, validation of the estimated thermodynamic properties of hydrocarbons in the confined spaces is still required.

Typical pore size distributions of shale reservoirs range in approximately 1–20 nm.(16) In such a confined space, interactions between rock and fluid molecules meaningfully affect fluid behavior and cause changes in fluid properties. Previous studies reported that the water mobility of confined water becomes significantly slower than that of bulk water under the same condition.(17)Moreover, Zarragoicoechea and Kuz(18) have shown that the shifts in the critical temperature are proportional to the size of the mesopore. Normally, as pore size decreases, the critical temperature and freezing/melting points tend to decrease.(19-21) Furthermore, pore size and the nature of the pore surface induce a shift in the phase diagrams, critical properties, and surface tension of confined fluids.(22) In our previous work, (23) we reported that both critical pressures and temperatures of pure components of hydrocarbon (methane and ethane) are reduced when the pore size decreases and the effect of confinement becomes less significant in

larger pores when the thermodynamic properties of the confined hydrocarbons approach the bulk properties.

Adsorption equilibria of nanoporous systems involve competition between molecules of different types. Several theories have been developed to describe mixture adsorption phenomena, such as the Langmuir theory,(24-26) the ideal adsorbed solution theory (IAST),(27) and molecular density-functional theory (DFT).(28, 29) Dong et al.(30) have studied the effect of capillary pressure and an adsorbed film on phase equilibria of confined pure components and their mixtures in nanopores of tight and shale rocks using the Peng–Robinson equation of state coupled with the capillary pressure equation and adsorption theory. This study showed that the presence of an adsorbed film can increase the vapor–liquid equilibrium constant (*K*-value) and cause a shift of bubble point pressure and dew point pressure of the mixtures. Furthermore, Tan and Piri(31) have performed a study of the phase equilibria of a confined fluid in nanopores using the perturbed-chain statistical association fluid theory equation of state (PC-SAFT EOS)/Laplace EOS and Vl method. In addition, molecular simulation has been used to help understand the competitive adsorption phenomena of mixtures in shale reservoirs. For example, microporous molecular models of kerogen were contructed using data from organic geochemistry experiments and Fourier transform infared (FTIR) spectroscopy and used in a molecular simulation study to examine methane/ethane adsorption in a shale reservoir.(32, 33) These results indicated the preferential sorption of ethane over methane, which aligned with an observation from sorption experiments of shale samples performed by Wang et al.(34)

Tan and Gubbins(35) have reported the selectivity of ethane relative to methane for a wide range of system parameters, such as temperature, pressure, bulk fluid composition, and pore size, using classical DFT solved within the nonlocal density approximation. Different types of selectivity isotherms were found at various system conditions. For example, the shape of selecitivy isotherms at temperatures below and above the critical temperature were characterized. While our previous work(23) was primarily focused on the effect of confinement on *PVT* properties of methane and ethane pure components, in this work, molecular simulations are used to observe the selectivity of ethane relative to methane in the slit-pore carbon that represents organic pores in a shale reservoir. Additionally, pressure–composition phase diagrams and critical properties of confined methane–ethane mixtures are calculated using classical molecular dynamics (MD) and grand canonical Monte Carlo (GCMC) simulations of kerogen modeled as slit pores with graphene walls representing different pore sizes. MD simulations are utilized to investigate the motion of methane and ethane as well as to evaluate their locations at equilibrium in nanoscale pores. GCMC simulations are used to determine methane–ethane mixture isotherms at various temperatures in order to examine adsorption selectivity and evaluate first-order phase transitions of the mixture. The p–x^{a}_{1}–y^{a}_{1} mixture phase

envelopes are obtained, where x^a_1 and y^a_1 are the mole fractions of liquid and vapor in the adsorbed phase, respectively.

Methodology

We focus on the phase behavior of methane–ethane mixtures in kerogen pores present in shale reservoirs. Kerogen is a mixture of organic materials arranged in stacks of aromatic-type macromolecules. The aromatic structures are composed of multiple elements, such as carbon (the largest proportion) but also hydrogen, oxygen, nitrogen, and sulfur. The proportion of each element and its chemical structure vary distinctively from sample to sample.(36) To simplify the problem, a slit graphite pore is used in molecular simulations to represent model kerogen pores in organic-rich shale reservoirs.

Force Fields

The Lennard-Jones (LJ) potential is a simple and popular model to approximate the van der Waals interactions between neutral particles:

$$u(r_{ij}) = 4\epsilon_{ij}\left[\left(\frac{\sigma_{ij}}{r_{ij}}\right)^{12} - \left(\frac{\sigma_{ij}}{r_{ij}}\right)^{6}\right] \quad (1)$$

ϵ_{ij} and σ_{ij} are the LJ potential parameters that characterize the molecular size and strength of the intermolecular interactions, and r_{ij} *i*s the distance between the centers of mass of the molecular pair. The LJ parameters are reported in Table 1. The optimized potential for liquid simulations (OPLS) model(37) is used for methane and ethane. The C–C parameters in graphite are from the work of Kurniawan et al.(38)

Table 1. LJ Potential Parameters

pair interaction	σ_{ii}, Å	ϵ_{ii}/k, K
CH_4–CH_4	3.730	148.0
CH_3–CH_3 (for ethane)	3.775	104.1
C–C	3.400	28.0

The LJ parameters for the unlike interactions are determined by the Lorentz–Berthelot combining rules:(39)

$$\sigma_{ij} = \frac{\sigma_{ii} + \sigma_{jj}}{2} \quad (2)$$

$$\epsilon_{ij} = \sqrt{\epsilon_{ii}\epsilon_{jj}} \quad (3)$$

Molecular Simulations

MD Simulations

MD simulations were performed at a fixed number of particles (*N*), volume (*V*), and temperature (*T*), i.e., in the canonical *NVT* ensemble. They were

primarily used to understand fluid behavior and interactions between fluid and nanoscale pores and to complement the GCMC results following the time evolution in selective environments of the confined system. The LJ interactions were truncated at $r_c = 5 \max(\sigma_{ij})$,(40) and a long-range correction was applied in the computation as implemented in the DL_Poly 2 software.(41) An initial configuration with a fluid composed of 50% methane molecules (blue) and 50% ethane molecules (red) is shown in Figure 1a. Graphene layers located in the middle of the simulation box create a restricted space, representing a pore, while the rest of the system represents the bulk phase. Periodic boundary conditions were used in the three spatial directions.

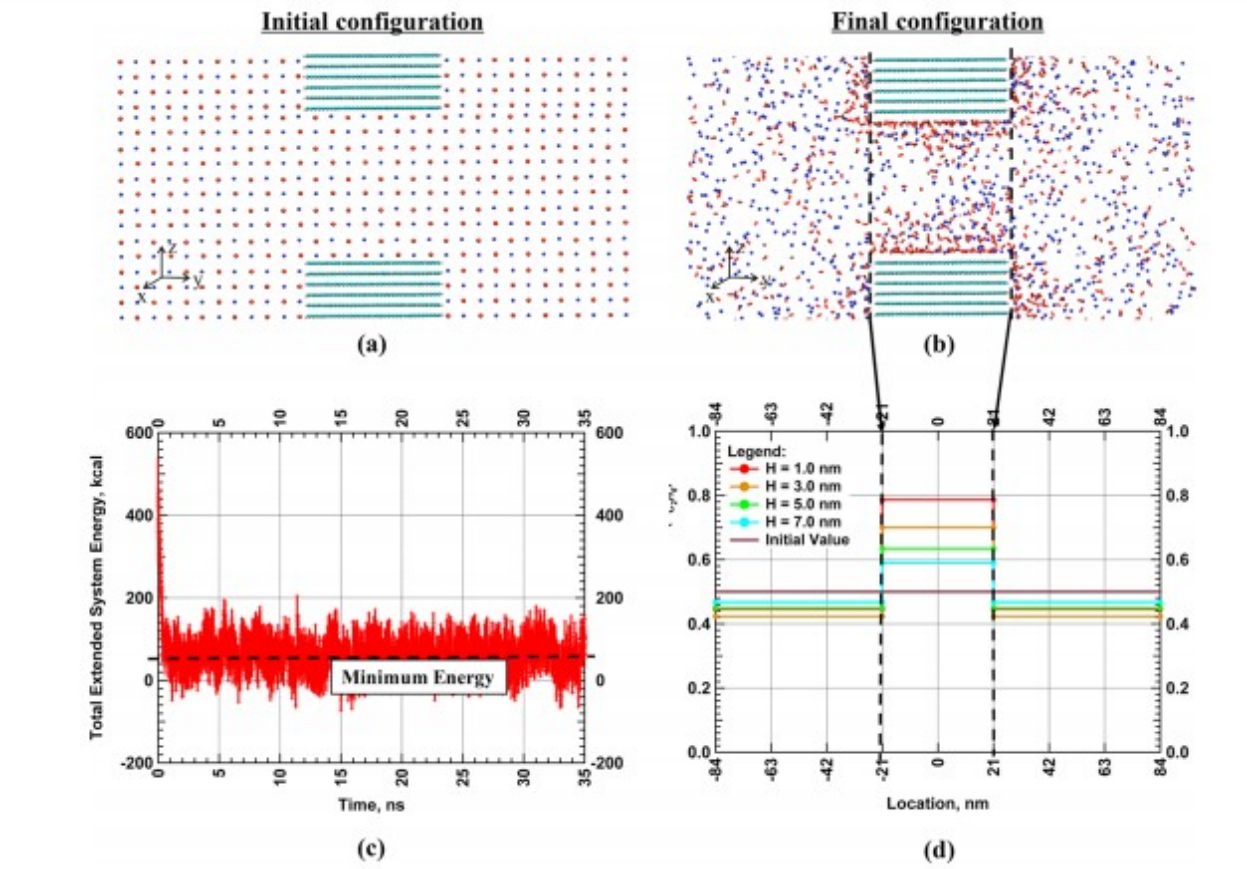

Figure 1. (a) Initial and (b) final configuration at t_s = 35 ns from classical MD simulation of a methane (blue)–ethane (red) mixture in a system containing a slit graphite pore with H = 5.0 nm and a bulk phase at T = 300 K. (c) Total extended system energy over simulation time. (d) Average ethane mole fraction profile in the y-direction of the mixture in different pore sizes.

Apart from LJ potential parameters in Table 1, additional basic inputs of MD simulations are summarized in Table 2.

Table 2. MD Simulation Details

simulation time (ns)	35
height (H) between pore layers (nm)	1, 3, 5, 7
temperature (K)	300
initial ethane mole fraction (bulk, confined)	0.5, 0.5
initial mixture density (bulk, confined) (g/cm^3)	0.177, 0.185
simulation cell dimensions	160.8 × 40.8 × 42 Å
pore structure dimensions	42 × 42 × H (variable depending on pore size)

GCMC Simulations

The GCMC simulation technique was applied to determine methane–ethane mixture isotherms at various conditions using the multipurpose simulation code MUSIC.(42) Consequently, the mixture isotherms were analyzed to understand the competitive adsorption of methane and ethane in the nanoscale pores and used to derive critical properties and phase envelopes of the confined methane–ethane mixtures in different pore sizes. As in MD simulations, the LJ interactions were truncated at $r_c = 5\ \max(\sigma_{ij})$, and periodic boundary conditions were used in the three spatial directions. This model was validated in our previous work(23) using experimental data of methane adsorption isotherms on thermally graphitized carbon black measured by Avgul and Kiselev.(43)Using the GCMC technique to evaluate the isotherms leads to a hysteresis depending on if the simulation is done at increasing or decreasing pressures. This means that the first-order transitions appear at different pressures if the phase space is examined by increasing or decreasing the pressure.(44-46) This is a well-known behavior that also has been detected experimentally.

Besides the LJ potential parameters in Table 1, additional basic inputs for GCMC simulations are summarized in Table 3.

Table 3. GCMC Simulation Details

number of steps	20 million
GCMC move types	insert, delete, translate, rotate
bulk fugacity evaluation	Peng–Robinson EOS[47]

Results and Discussion

Selectivity of Specific Species in Nanopores

MD simulations were used to characterize the selectivity of the confined system toward specific species. As mentioned in the previous section, the initial configuration contains a mixture with 50% methane and 50% ethane in both slit graphite pore and the bulk phase (Figure 1a). The separation between the graphene layers is varied from 1.0 to 7.0 nm to study the effect of confinement. The temperature of the system is 300 K and the total simulation time is 35 ns. An example of the final configuration, the case of H

= 5.0 nm, is shown in Figure 1b. The variation of the total energy versus simulation time is depicted Figure 1c. The average mole fraction of ethane, x_{C2H6}, for each interval is computed and graphed over the *y*-direction, as shown in Figure 1d. It can be observed that although the initial ethane mole fraction of fluid for all intervals of the system (including both the pore and the bulk segments) is equal to 0.5, the instantaneous ethane mole fraction at each interval changes and varies throughout the system. For instance, the last configuration shows that the ethane mole fraction in the slit pore region (the area between the two dashed lines in Figure 1d) for all the cases is greater than 0.5, and consequently, the ethane mole fraction in the bulk phase is lower than 0.5. Moreover, the ethane mole fraction in the smaller pore is greater than that in the larger pore, even though the starting condition of each case is the same. For instance, at t = 35 ns, the average mole fractions of ethane in the pores with H = 1.0, 3.0, 5.0, and 7.0 are 0.79, 0.70, 0.63, and 0.59, respectively. According to the mole fraction profiles in the *y*-direction (see Figure 1d), the difference of the ethane mole fraction between the slit pore segment and the bulk segment is larger for a smaller pore, and the profile turns out to fluctuate less for larger pores as the ethane mole fraction inside the pore approaches 0.5, the average value of the total system. This implies that, as the pore size increases, the influence of the interactions between the fluid molecules and the pore walls becomes less significant upon fluid behavior and properties, so that the fluid compositions in the slit pore segment and the bulk become similar.

In addition, MD simulations were used to investigate the fluid exchange between the bulk and pore regions. Figure 2 illustrates changes of the configuration over time from t = 0 to 35 ns for the case of H = 5.0 nm. Again, at t = 0 ns, the mole fractions of methane and ethane are the same, and the average density of the mixture is approximately 0.11 g/cm^3 for both regions. After the simulation starts, fluid molecules moved inside the slit pore due to interactions between fluid molecules and the pore wall. As a result, the differences of the average mixture density and the fluid's composition between the bulk and pore can be observed. The mixture density in the pore region increases to 0.212 g/cm^3 at t = 35 ns, while that in the bulk region decreases to 0.089 g/cm^3 at t = 35 ns (see Figure 3a). This implies that the fluid molecules tend to accumulate or be adsorbed inside the pore rather than staying in the gas phase. The changes of ethane mole fraction in pore and bulk over time are illustrated in Figure 3b. The ethane mole fraction in the pore fluctuates between 0.61 and 0.64 from t = 2 to 35 ns. This can lead to the conclusion that ethane is preferred over methane in the confined system.

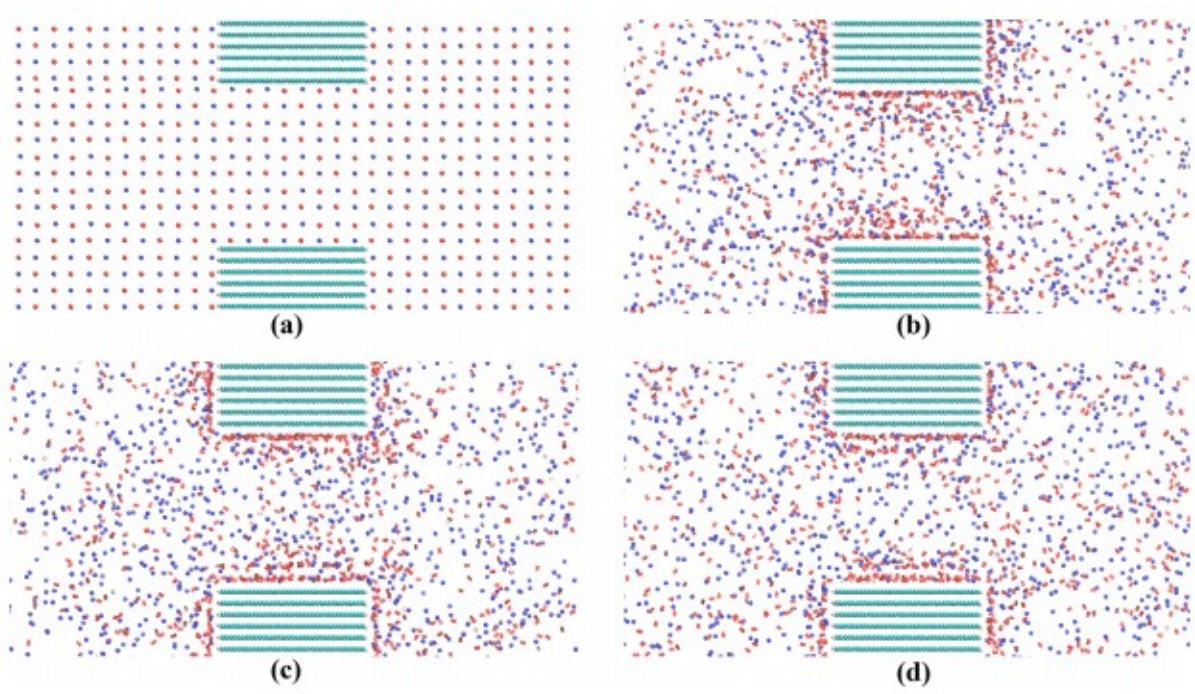

Figure 2. Configurations from classical MD simulation of a methane (blue)–ethane (red) mixture in a system containing a slit graphite pore with H = 5.0 nm and a bulk phase at T = 300 K at (a) t = 0 ns, (b) t = 2 ns, (c) t = 10 ns, and (d) t = 35 ns.

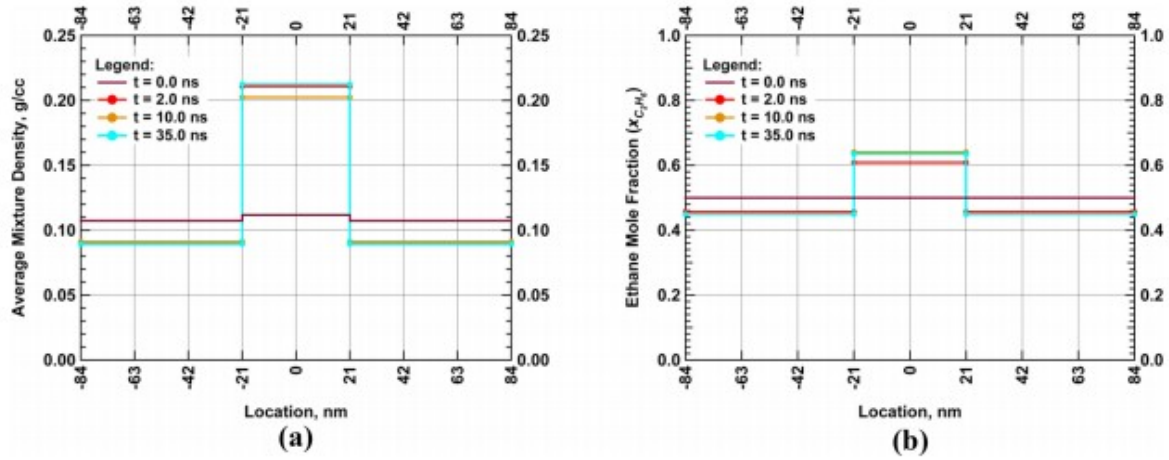

Figure 3. (a) Average mixture density and (b) ethane mole fraction of a methane–ethane mixture in a system containing a slit graphite pore with H = 5.0 nm at T = 300 K from t = 0 to 35 ns.

The preference for ethane shown in Figures 1 and 3 can be characterized by the selectivity, defined as the ratio of mole fractions in the adsorbed pore divided by the ratio of mole fractions in the bulk mixture.(35, 48) The selectivity of ethane over methane is computed as follows:

$$S_{C_2/C_1} = \frac{x_{\text{confined},C_2H_6}/x_{\text{confined},CH_4}}{x_{\text{bulk},C_2H_6}/x_{\text{bulk},CH_4}} \qquad (4)$$

The parameters used to calculate the selectivity can be derived from isotherms obtained from GCMC simulations. For a binary mixture system, the GCMC method is used to determine not only the equilibrium density of the confined fluid at the given pressure and temperature but also the fluid's composition in the confined system at equilibrium. Again, the isotherm of the confined system obtained from the GCMC simulation must satisfy the following equations:

$$\mu_{\text{bulk,CH}_4}^{\text{vapor}}(T,p) = \mu_{\text{confined,CH}_4}^{\text{vapor}} = \mu_{\text{confined,CH}_4}^{\text{liquid}} \quad (5)$$

$$\mu_{\text{bulk,C}_2\text{H}_6}^{\text{vapor}}(T,p) = \mu_{\text{confined,C}_2\text{H}_6}^{\text{vapor}} = \mu_{\text{confined,C}_2\text{H}_6}^{\text{liquid}} \quad (6)$$

The amounts of each type of fluid molecules in the confined system are dependent on the interaction between the sorbent (slit graphite pore) and the sorbate (methane and ethane). Since the interactions between the pore wall and those of the individual fluid molecules are different, this event causes a selective environment in the pore, and the system tends to adsorb one fluid more than the other.

The GCMC simulation was set up (as illustrated in Figure S1 of the Supporting Information) to study the trends of selectivity as a function of temperature. The reservoir pressure and bulk ethane mole fraction are fixed at 5 MPa and 0.5, respectively. The reservoir temperature was varied from 300 to 400 K. It can be observed that the selectivity tends to decrease as temperature increases, as shown in Figure 4. This implies that the confined system becomes less selective at higher temperatures. Figure 5 illustrates the selectivity as a function of the reservoir (bulk) pressure at a temperature of 400 K and an ethane mole fraction of 0.5 in the bulk. The reservoir pressure is varied from 200 kPa to 6.2 MPa. It is noticeable that the selectivity tends to decrease as the reservoir pressure increases. For this example, the confined fluid remains single phase at the given conditions. As a result, the trend of the selectivity was continuous. However, at a phase transition, the discontinuity of the trend may occur, and we can apply this concept to derive the pressure–composition (p–x) diagram of the binary mixture in a confined space. In both scenarios, the selectivity of ethane over methane is greater than unity, meaning that ethane is preferred to methane in the confined system. As the pore size increases, the selectivity decreases and approaches unity. Here, the fluid compositions of the bulk and confined mixtures are identical, as expected, since the effect of the interaction between the fluid molecules and the pore walls becomes less significant. These observations are in agreement with those reported by Tan and Gubbins.(35)

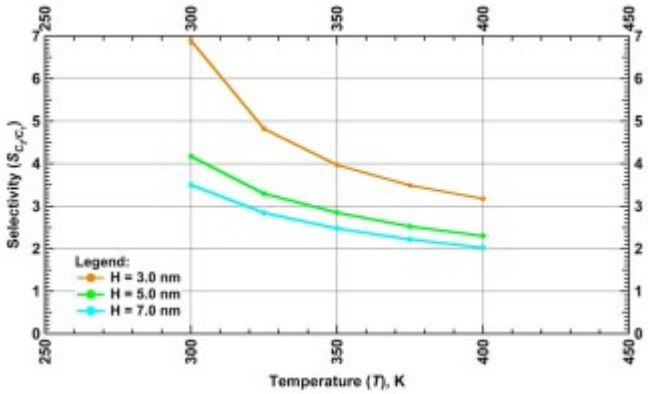

Figure 4. Selectivity as a function of temperature in different pore sizes at p = 5.0 MPa and $x_{bulk,C2H6}$ = 0.5.

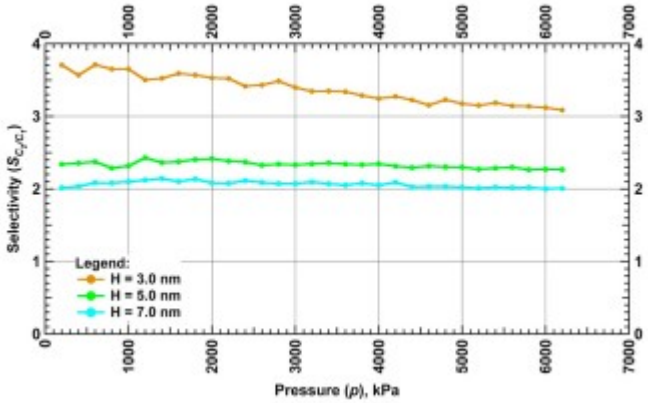

Figure 5. Selectivity as a function of pressure in different pore sizes at T = 400 K and $x_{bulk,C2H6}$ = 0.5.

Phase Diagram of Confined Methane–Ethane Mixtures

In the preceding section, the interactions between the fluid molecules and the pore walls caused deviations of fluid composition in the confined space. For the studied pore system, ethane was preferred to methane. This selective environment may cause shifts of the phase diagrams in the confined space. The selectivity is a function of the reservoir (bulk) temperature, pressure, bulk fluid composition, pore–fluid and fluid–fluid interactions, and pore size.

In the previous section, we also observed continuity of the trend of selectivity over the pressure range at different pore sizes. We mentioned that this might not hold when the condition is close to a first- or second-order phase transition. To prove this statement, GCMC simulations were used to determine the isotherms of methane and ethane in the slit graphite pore with H = 5.0 nm, T = 240 K, and $x_{bulk,C2H6}$ = 0.35 (see Figure 6a). The bulk pressure is varied from 2.75 to 4.25 MPa by increments of 50 kPa. At low pressure, the fluid mixture is in the vapor phase. At $p \approx$ 3.65–3.7 MPa, a jump is observed in the isotherms. This jump represents a first-order phase transition, the change of state from liquid to vapor or vice versa of the mixture. The mole fraction of ethane in the confined mixture over the

pressure range is computed and plotted in Figure 6b. From the plot, it is observed that the ethane mole fraction of the confined mixture in the vapor phase is almost constant, around 0.59. Similarly, the ethane mole fraction of the confined mixture in the liquid phase is almost constant, around 0.66. At the phase transition, a jump of the ethane mole fraction can be detected. This is because, at the phase transition, the equilibrium ethane mole fractions of the vapor and liquid phases are different, and the discontinuity of the trend of selectivity or ethane mole fraction of the confined mixture occurs. This concept is applied to derive *p*–*x* diagrams of confined binary mixtures, as explained below. The selectivity of the mixture in the vapor phase and liquid phase are approximately 8.2 and 11.4. Thus, at this condition, the selectivity jumps from 8.2 to 11.4 at the phase transition. This proves that the selectivity of the slit graphite pore with H = 5.0 nm varies as a function of the bulk pressure.

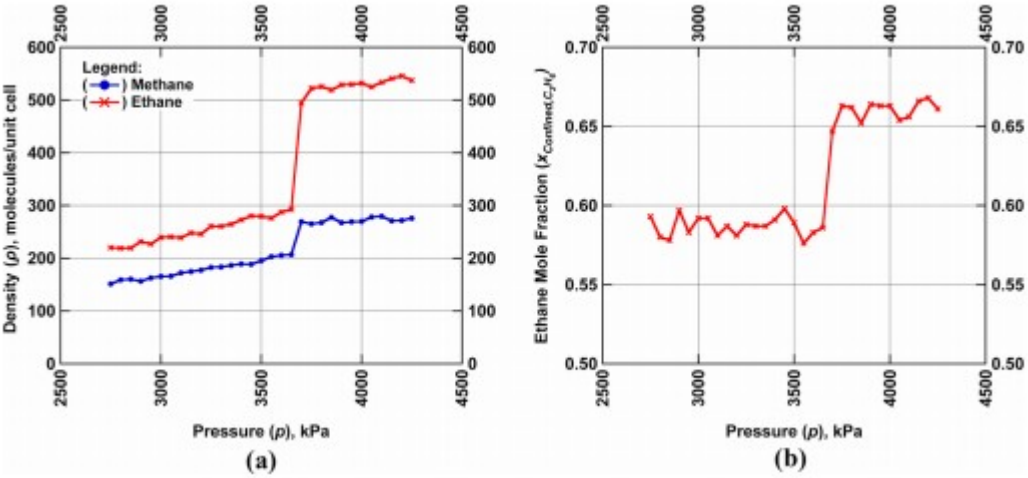

Figure 6. (a) Isotherms of methane and ethane and (b) ethane mole fraction of the confined mixture in the slit graphite pore with H = 5.0 nm at T = 240 K and $x_{bulk,C2H6}$ = 0.35.

Figure 7a depicts isotherms of methane and ethane in the slit graphite pore with H = 5.0 nm at T = 240 K and $x_{bulk,C2H6}$ = 0.15. At this condition, the mixture is a supercritical fluid. The bulk pressure is varied from 4 to 5.5 MPa by increments of 50 kPa. It is observed that the fluid density increases when the pressure increases. However, a first-order first transition cannot take place in this case, since the fluid is in the supercritical condition. The mole fraction of ethane in the confined mixture over the pressure range is shown in Figure 7b. From the graph, it is observed that the ethane mole fraction increases continuously over the pressure range. This differs from the previous case, where there is a discontinuity at the phase transition. The selectivity gradually increases from 8.2 at p = 4 MPa to 9.6 at p = 5.5 MPa. Again, this proves that the selectivity of a slit graphite pore with H = 5.0 nm varies as a function of the bulk pressure. At the same bulk pressure, the selectivity of this case is lower than that of the previous case ($x_{bulk,C2H6}$ = 0.35). For example, at p= 4.2 MPa, the selectivity of the previous case is equal to 11.4, which is higher than the selectivity of 8.2 from this case.

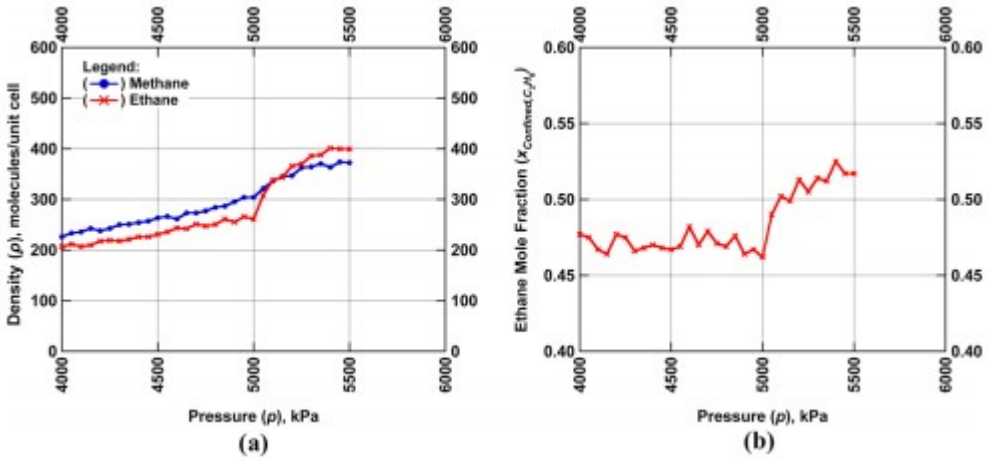

Figure 7. (a) Isotherms of methane and ethane and (b) ethane mole fraction of the confined mixture in a slit graphite pore with H = 5.0 nm at T = 240 K and $x_{bulk,C2H6}$= 0.15.

Similar to Tan and Gubbins' observation,(35) the selectivity isotherms differ depending on confined fluid condition. When the confined fluid is below the critical point, a vertical jump in the isotherms occurs at a gas–liquid phase transition (Figure 6). On the other hand, when the confined fluid is in supercritical condition, the isotherms increase steadily with pressure (Figure 7). We applied this knowledge to derive new phase diagrams and critical properties of a hydrocarbon mixture, as shown in Figure 8.

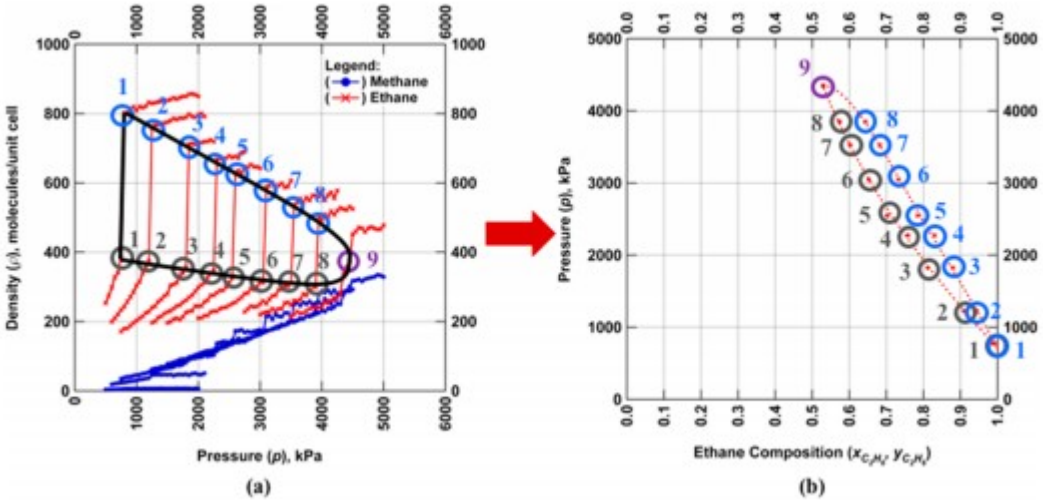

Figure 8. (a) Isotherms of the methane–ethane mixture in a slit graphite pore with 5.0 nm of separation at T = 240 K and (b) the p–x diagram of the mixture corresponding to the isotherms.

The phase diagram and critical properties of a hydrocarbon mixture were calculated after determining phase transitions of mixtures with different compositions. According to the isotherms of the confined mixture shown in Figure 6, the equilibrium composition of the confined fluid is a two-phase mixture having ethane in vapor ($y_{confined,C2H6}$) (59%) and liquid ($x_{confined,C2H6}$) phases (66%). These results indicate that the original gas mixture splits into two phases that are rich in ethane. Multiple scenarios of this type of

simulation with different fluid compositions were used to generate a *p*–*x* diagram (pressure–composition) for a mixture. Once isotherms for each component are found, the fluid composition in the vapor and liquid phases at the saturation pressure of the mixture can be computed. Consequently, these data are used to create a phase diagram and obtain a critical point of the mixture. Figure 8a illustrates isotherms of a methane–ethane mixture indicating a phase transition in a slit graphite pore with 5.0 nm of separation for different fluid compositions at $T = 240$ K. At the given temperature, the isotherms of the confined mixture are distinct for each individual bulk fluid composition, and each isotherm yields a different bubble point pressure and dew point pressure. Mole fractions of ethane at the bubble point pressure and dew point pressure of each isotherm were calculated (no. 1–8) and plotted in the *p*–*x* diagram to generate bubble point and dew point lines. At critical condition, the isotherm of the confined mixture must be continuous, and the ethane mole fraction and pressure at the critical point can be read from the inflection point of the isotherm (no. 9). Figure 8b is a complete *p*–*x*diagram of confined methane–ethane mixtures at the constant temperature of 240 K. The critical point, shown as the purple circle, can be seen in Figure 8a,b. The critical locus curve was obtained by connecting the critical points of *p*–*x* diagrams at different temperatures. It is used to approximate critical properties of a mixture as a function of overall fluid composition.

In our previous study,(23) it was shown that the effect of confinement caused the reduction in the critical temperature and pressure of pure components of confined methane and ethane in slit graphite pores. For confined methane–ethane mixtures, interactions between the pore walls and the fluid molecules also affect the shape of the mixture phase envelope and critical properties, such as the critical locus curve. Figure 9a illustrates a bulk phase diagram of a methane–ethane mixture derived from experimental data from Bloomer et al.(49) The diagram contains a collection of the mixture phase envelopes (*p*–*x* diagram) at different temperatures. Connecting the critical points of each envelope yields a critical locus curve, as shown by the maroon line in the plot. The area above the curve is the supercritical region. The intersections between the curve and the *y*-axis at $x_{\mathrm{bulk,C2H6}} = 0$ and $x_{\mathrm{bulk,C2H6}} = 1$ are the critical pressures of bulk methane and ethane, respectively. Bulk critical properties of the mixture at a specified composition can be estimated from this plot.

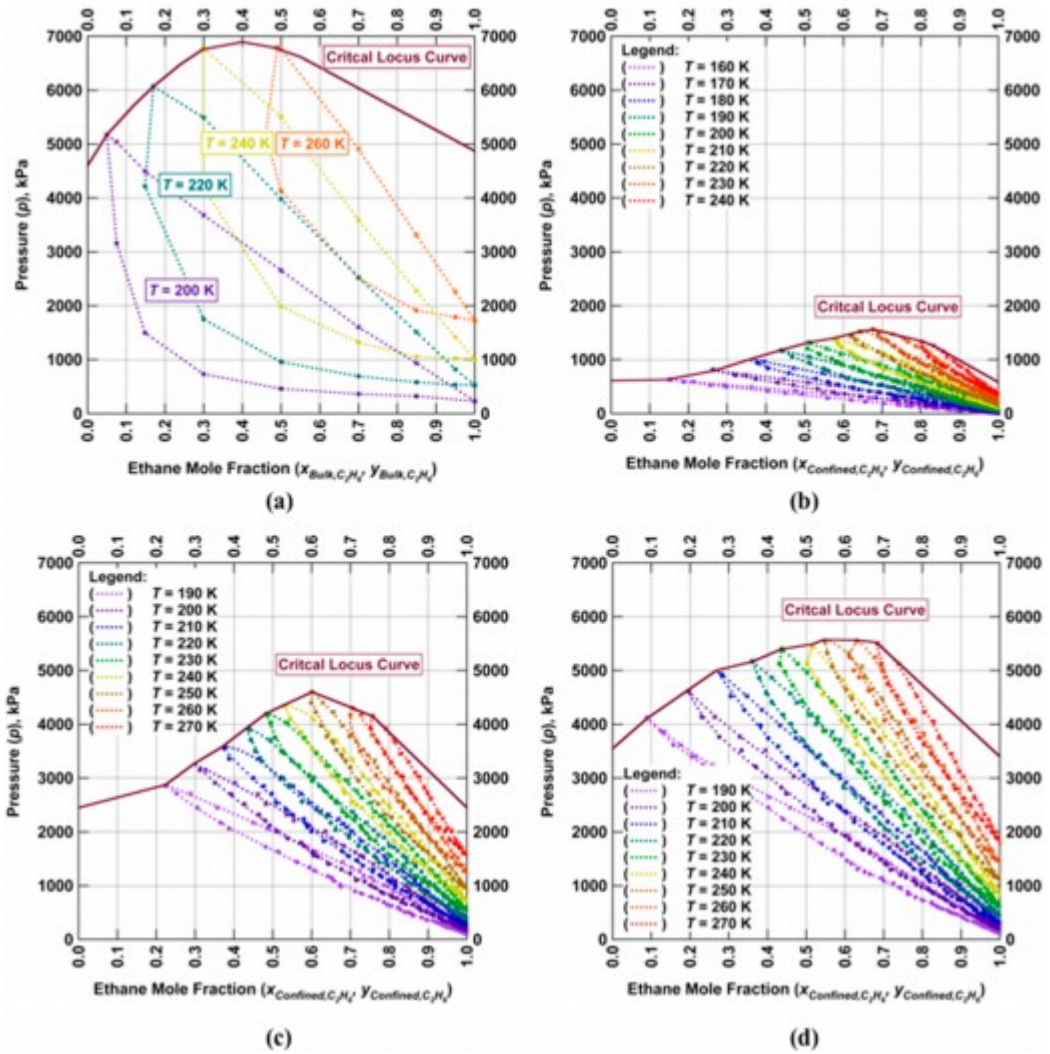

Figure 9. Comparison of (a) the bulk methane–ethane mixture phase diagram(49)and that of the confined mixture in the slit pore with (b) H = 3.0 nm, (c) H = 5.0 nm,(23) and (d) H = 7.0 nm.

A phase diagram of the confined mixture in a slit graphite pore with 3.0, 5.0, and 7.0 nm of separation was generated as illustrated in parts b, c, and d of Figure 9, respectively. A series of phase envelopes of the confined mixture was obtained from the GCMC simulations using the described procedures. For H = 3.0 nm, the phase envelopes are generated from T = 160 to 240 K, which fall between the critical temperatures of the confined methane (155 K) and ethane (258 K). For H = 5.0 nm, the phase envelopes are generated from T = 190 to 270 K, which is between the critical temperatures of the confined methane (175 K) and ethane (292 K). For H = 7.0 nm, the phase envelopes are generated from T = 190 to 270 K, which is between the critical temperatures of the confined methane (181.5 K) and ethane (300 K). Again, the intersections between the critical locus curve and the y-axis at $x_{\text{confined,C2H6}}$ = 0 and $x_{\text{confined,C2H6}}$ = 1 are the critical pressures of confined methane and ethane, respectively.

It is observed that, at the same temperature, the shapes and magnitudes of the bulk and the confined phase envelopes change dramatically because of the restricted environment existent in kerogen pores of shale reservoirs. Furthermore, the subsequent shift of the critical locus curve of the mixture is in the direction of lower critical temperature and pressure, as similarly observed with the pure components.

In addition, the critical locus curve of the confined mixture in the smaller pore is lower than that in the larger pore. This means that for the same fluid composition, the critical pressure of the confined mixture in the smaller pore is lower than that in the larger pore. The *p*–*x* diagram also shows that the critical temperature decreases as the pore size decreases. For example, at x_{C2H6} = 0.5, the critical pressure of a bulk methane–ethane mixture is approximately 6.8 MPa, whereas that of the confined mixture in a slit pore with H = 7.0, 5.0, and 3.0 nm is around 5.4, 4.3, and 1.3 MPa, respectively. Likewise, at x_{C2H6} = 0.5, the critical temperature of a bulk methane–ethane mixture is approximately 263 K, whereas that of the confined mixture in a slit pore with H = 7.0, 5.0, and 3.0 nm is around 239, 232, and 199 K, respectively.

The magnitude of critical properties of the confined mixture decreases rapidly when the pore size reduces from 5.0 to 3.0 nm. As the pore size increases, the critical locus curve of the confined mixture becomes closer to that of the bulk mixture, as expected.

Figure 10 illustrates a comparison of *p*–*T* diagrams for a binary methane–ethane mixture with a methane mole fraction of 30.02% and ethane mole fraction of 69.98% in the bulk phase—from reported experimental data(49)—and that in a slit graphite pore with a 3.0, 5.0, and 7.0 nm of separation. It is observed that the shape and area of the confined mixture phase enveloped are different from those of the bulk mixture and that the critical point of the confined mixture shifts from the bulk critical point. Both critical pressure and temperature are reduced in the small pore. The critical pressure and temperature of the bulk mixture are 6.2 MPa and 281 K. In comparison, the critical pressure and temperature of the confined mixture are 5.5 MPa and 273 K for H = 7.0 nm, 4.0 MPa and 260 K for H = 5.0 nm, and 1.5 MPa and 232 K for H = 3.0 nm.

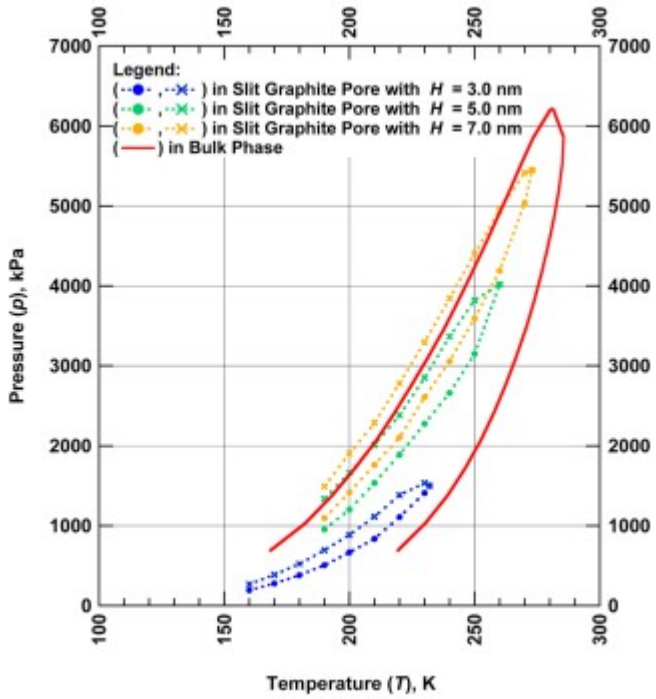

Figure 10. Comparison of *p*–*T* diagrams for a binary methane–ethane mixture with a methane mole fraction of 30.02% and ethane mole fraction of 69.98% in the bulk phase and in a slit graphite pore with 5.0 nm of separation.

The confined mixture has a higher dew point pressure than the bulk mixture with the same fluid composition, while the bubble point pressure of the confined mixture may be either lower or higher than that of the bulk mixture, depending on the temperature. The shift of the phase diagram of the confined mixture implies changes of fluid properties in a confined system, such as kerogen pores in a shale reservoir. As a result, using conventional EOS may yield errors in the calculation of fluid properties in shale reservoirs.

Conclusions

The interactions between fluid molecules and the pore walls create a selective environment in the confined space. As we observed from the GCMC and classical MD simulation results, the slit graphite pore representing a kerogen pore in a shale reservoir prefers to adsorb a heavier component, i.e., ethane, more than a lighter component, i.e., methane. The selectivity of the pore toward ethane tends to decrease when the temperature increases. Furthermore, selectivity varies when the reservoir (bulk) pressure and the bulk fluid composition change. As the pore size increases, the selectivity decreases and approaches unity, where the fluid composition of the confined mixture and bulk mixture are identical.

These simulations were used to generate *p*–*x* diagrams, and a phase envelope was created from a collection of *p*–*x* diagrams. The effect of confinement causes deviations of the shapes and magnitudes of phase diagrams from the bulk. The critical properties and the phase envelope

shapes are substantially different from those of the bulk mixture. As the pore size decreases, both critical pressure and temperature tend to decrease, as similarly observed with the pure component. As the pore size increases, the critical locus curve of the confined mixture rises and approaches the bulk curve, since there is less influence from the effect of confinement.

According to the *p*–*T* diagrams, both the critical pressure and temperature of the confined mixture are lower than those of the bulk fluid. The confined mixture has a higher dew point pressure than the bulk mixture with the same fluid composition. The bubble point pressure of the confined mixture may be either lower or higher than that of the bulk mixture, depending on the temperature.

On the basis of these observations, the fluid composition of the produced hydrocarbon mixture may not be a good representation of the original fluid in the reservoir. The mole fraction of the heavy component of the contained mixture is higher than that of the produced fluid. At the beginning of production, shale reservoirs tend to release lighter components (i.e., methane) and the heavier components are left behind. Once the lighter components are almost completely drained from the shale reservoirs, the reservoirs will start releasing the heavier components. This phenomenon may cause changes in the produced fluid composition over the production time.

Future work will include improved molecular modeling of the kerogen pores by adding functional groups containing oxygen, nitrogen, and sulfur to graphite sheet.(50, 51) In addition to their effect of confinement, such functional groups may influence the phase behavior of hydrocarbon mixture in kerogen pores in organic-rich shale resevoirs.

References

(1) Elgmati, M. Shale Gas Rock Characterization and 3D Submicron Pore Network Reconstruction. Masters Thesis, Missouri University of Science and Technology, 2011; Paper 6735. (2) Hu, Y.; Devegowda, D.; Striolo, A.; Civan, F.; Sigal, R. F. Microscopic Dynamics of Water and Hydrocarbon in Shale-Kerogen Pores of Potentially Mixed-Wettability. Presented at the 2013 SPE Unconventional Resources Conference∂Canada, Calgary, Canada, 2013; Paper SPE 167234. (3) Moore, E. B.; de la Llave, E.; Welke, K.; Scherlis, D. A.; Molinero, V. Freezing, Melting and Structure of Ice in A Hydrophilic Nanopore. Phys. Chem. Chem. Phys. 2010, 12, 4124−4134. (4) Lö hr, S. C.; Baruch, E. T.; Hall, P. A.; Kennedy, M. J. Is Organic Pore Development in Gas Shales Influenced by The Primary Porosity and Structure of Thermally Immature Organic Matter? Org. Geochem. 2015, 87, 119−132. (5) Wang, M.; Yang, J.; Wang, Z.; Lu, S. Nanometer-Scale Pore Characteristics of Lacustrine Shale, Songliao Basin, NE China. PLoS One 2015, 10, e0135252. (6) Clarkson, C. R.; Haghshenas, B. Modeling of Supercritical Fluid Adsorption on Organic-Rich Shales and Coal. Presented at the 2013 SPE Unconventional Resources Conference∂USA, The Woodlands, TX, 2013; Paper SPE 164532. (7) Moridis,

G. J.; Blasingame, T. A. Evaluation of Strategies for Enhancing Production of Low-Viscosity Liquids from Tight/Shale Reservoirs. Presented at the 2014 Latin American and Caribbean Petroleum Engineering Conference, Maracaibo, Venezuela, 2014; Paper SPE 169479. (8) Shabro, V.; Torres-Verdin, C.; Javadpour, F. Numerical Simulation of Shale-Gas Production: From Pore-Scale Modeling of Slip-Flow, Knudsen Diffusion, and Langmuir Desorption to Reservoir Modeling of Compressible Fluid. Presented at the 2011 SPE North American Unconventional Gas Conference and Exhibition, The Woodlands, TX, 2011; Paper SPE 144355. (9) Ambrose, R. J.; Hartman, R. C.; Akkutlu, I. Y. Multi-Component Sorbed Phase Considerations for Shale Gas-in-Place Calculations. Presented at the 2011 SPE Production and Operations Symposium, Oklahoma City, OK, 2011; Paper SPE 141416. (10) Ambrose, R. J.; Hartman, R. C.; Diaz-Campos, M.; Akkutlu, I. Y.; Sondergeld, C. H. Shale Gas-In-Place Calculations Part I: New Pore-Scale Considerations. Soc. Petrol Eng. J. 2012, 17, 219−229. (11) Das, M.; Jonk, R.; Schelble, R. Effect of Multicomponent Adsorption/Desorption Behavior on Gas-in-Place (GIP) and Estimated Ultimate Recovery (EUR) in Shale Gas Systems. Presented at the 2012 SPE Annual Technical Conference and Exhibition, San Antonio, TX, 2012; Paper SPE 159558. (12) Sandoval, D. R.; Yan, W.; Michelsen, M. L.; Stenby, E. H. The Phase Envelope of Multicomponent Mixtures in The Presence of A Capillary Pressure Difference. Ind. Eng. Chem. Res. 2016, 55, 6530− 6538. (13) Freeman, C. M. A Numerical Study of Microscale Flow Behavior in Tight Gas and Shale Gas. Presented at the 2010 SPE International Student Paper Contest at the SPE Annual Technical Conference and Exhibition, Florence, Italy, 2010; Paper SPE 141125- STU. (14) Darabi, H.; Ettehad, A.; Javadpour, F.; Sepehrnoori, K. Gas Flow in Ultra-Tight Shale Strata. J. Fluid Mech. 2012, 710, 641−658. (15) Fathi, E.; Tinni, A.; Akkutlu, I. Y. Shale Gas Correction to Klinkenberg Slip Theory. Presented at the Americas Unconventional Resources Conference, Pittsburgh, PA, 2012; Paper SPE 154977. (16) Nagarajan, N. R.; Honarpour, M. M.; Arasteh, F. Critical Role of Rock and Fluid∂Impact on Reservoir Performance on Unconventional Shale Reservoirs. Presented at the 2013 Unconventional Resources Technology Conference, Denver, CO, 2013; Paper SPE 168864. (17) Hirunsit, P.; Balbuena, P. B. Effects of Confinement on Water Structure and Dynamics: A Molecular Simulation Study. J. Phys. Chem. C 2007, 111, 1709−1715. (18) Zarragoicoechea, G. J.; Kuz, V. A. Critical Shift of A Confined Fluid in A Nanopore. Fluid Phase Equilib. 2004, 220, 7−9. (19) Vishnyakov, A.; Piotrovskaya, E. M.; Brodskaya, E. N.; Votyakov, E. V.; Tovbin, Y. K. Critical Properties of Lennard-Jones Fluids in Narrow Slit-Shaped Pores. Langmuir 2001, 17, 4451−4458. (20) Kanda, H.; Miyahara, M.; Higashitani, K. Triple point of Lennard-Jones fluid in slit nanopore: Solidification of Critical Condensate. J. Chem. Phys. 2004, 120, 6173. (21) Moore, E. B.; de la Llave, E.; Welke, K.; Scherlis, D. A.; Molinero, V. Freezing, Melting and Structure of Ice in A Hydrophilic Nanopore. Phys. Chem. Chem. Phys. 2010, 12, 4124−4134. (22) Singh, S. K.; Sinha, A.; Deo, G.; Singh, J. K. Vapor-Liquid Phase Coexistence, Critical Properties, and Surface Tension of Confined

Alkanes. J. Phys. Chem. C 2009, 113, 7170−7180. (23) Pitakbunkate, T.; Balbuena, P. B.; Moridis, G. J.; Blasingame, T. A. Effect of Confinement on Pressure/Volume/Temperature Properties of Hydrocarbons in Shale Reservoirs. SPE J. 2016, 21, 621−634. (24) Markham, E. C.; Benton, A. F. The Adsorption of Gas Mixtures by Silica. J. Am. Chem. Soc. 1931, 53, 497−507. (25) Bai, R.; Yang, R. T. Thermodynamically Consistent Langmuir Model for Mixed Gas Adsorption. J. Colloid Interface Sci. 2001, 239, 296−302. (26) Bai, R.; Deng, J.; Yang, R. T. Improved Multisite Langmuir Model for Mixture Adsorption Using Multiregion Adsorption Theory. Langmuir 2003, 19, 2776−2781. (27) Myers, A. L.; Prausnitz, J. M. Thermodynamics of Mixed-Gas Adsorption. AIChE J. 1965, 11, 121−127. (28) Liu, Y.; Liu, H.; Hu, Y.; Jiang, J. Density Functional Theory for Adsorption of Gas Mixtures in Metal-Organic Frameworks. J. Phys. Chem. B 2010, 114, 2820−2827. (29) Tarazona, P.; Marini Bettolo Marconi, U.; Evans, R. Phase Equilibria of Fluid Interfaces and Confined Fluids: Non-Local Versus Local Density Functionals. Mol. Phys. 1987, 60, 573−595. (30) Dong, X.; Liu, H.; Hou, J.; Wu, K.; Chen, Z. Phase Equilibria of Confined Fluids in Nanopores of Tight and Shale Rocks Considering The Effect of Capillary Pressure and Adsorption Film. Ind. Eng. Chem. Res. 2016, 55, 798−811. (31) Tan, S. P.; Piri, M. Y. Retrograde Behavior Revisited: Implications for Confined Fluid Phase Equilibria in Nanopores. Phys. Chem. Chem. Phys. 2017, 19, 18890−18901. (32) Collell, J.; Galliero, G.; Gouth, F.; Montel, F.; Pujol, M.; Ungerer, P.; Yiannourakou, M. Molecular Simulation and Modelisation of Methane/Ethane Mixtures Adsorption onto a Microporous Molecular Model of Kerogen Under Typical Reservoir Conditions. Microporous Mesoporous Mater. 2014, 197, 194−203. (33) Huang, L.; Ning, Z.; Wang, Q.; Qi, R.; Li, J.; Zeng, Y.; Ye, H.; Qin, H. Thermodynamic and Structural Characterization of Bulk Organic Matter in Chinese Silurian Shale: Experimental and Molecular Modeling Studies. Energy Fuels 2017, 31, 4851−4865. (34) Wang, Y. T.; Tsotsis, T. T.; Jessen, K. Competitive Sorption of Methane/Ethane Mixtures on Shale: Measurements and Modeling. Ind. Eng. Chem. Res. 2015, 54, 12187−12195. (35) Tan, Z.; Gubbins, K. E. Selective Adsorption of Simple Mixtures in Slit Pores: A Model of Methane-Ethane Mixtures in Carbon. J. Phys. Chem. 1992, 96, 845. (36) Vandenbroucke, M. Kerogen: from Types to Models of Chemical Structure. Oil Gas Sci. Technol. 2003, 58, 243−269. (37) Jorgensen, W. L.; Madura, J. D.; Swenson, C. J. Optimized Intermolecular Potential Functions for Liquid Hydrocarbons. J. Am. Chem. Soc. 1984, 106, 6638−6646. (38) Kurniawan, Y.; Bhatia, S. K.; Rudolph, V. Simulation of Binary Mixture Adsorption of Methane and CO2 at Supercritical Conditions in Carbons. AIChE J. 2006, 52, 957−967. (39) Allen, M. P.; Tildesley, D. J. Computer Simulation of Liquids; Oxford University Press: Oxford, 1987. (40) Mecke, M.; Winkelmann, J.; Fischer, J. Molecular Dynamics Simulation of The Liquid-Vapor Interface: The Lennard-Jones Fluid. J. Chem. Phys. 1997, 107, 9264−9270. (41) Smith, W.; Forester, T. R. DL_POLY_2.0: A general-Purpose Parallel Molecular Dynamics Simulation Package. J. Mol. Graphics 1996, 14, 136−141. (42) Gupta, A.; Chempath, S.; Sanborn, M.; Clark, L.; Snurr, R. Object-Oriented Programming Paradigms for Molecular

Modeling. Mol. Simul. 2003, 29, 29−46. (43) Avgul, N. N.; Kiselev, A. V. Physical Adsorption of Gases and Vapors on Graphitized Carbon Blacks. Chem. Phys. Carbon 1970, 6, 1−124. (44) Diao, R.; Fan, C.; Do, D. D.; Nicholson, D. On The 2DTransition, Hysteresis and Thermodynamic Equilibrium of Kr Adsorption on A Graphite Surface. J. Colloid Interface Sci. 2015, 460, 281−289. (45) Sliwinska-Bartkowiak, M.; Gras, J.; Sikorski, R.; Radhakrishnan, R.; Gelb, L.; Gubbins, K. E. Phase Transitions in Pores: Experimental and Simulation Studies of Melting and Freezing. Langmuir 1999, 15, 6060−6069. (46) Klomkliang, K.; Do, D. D.; Nicholson, D. On The Hysteresis and Equilibrium Phase Transition of Argon And Benzene Adsorption in Finite Slit Pores: Monte Carlo vs. Bin-Monte Carlo. Chem. Eng. Sci. 2013, 87, 327−337. (47) Peng, D. Y.; Robinson, D. B. A New Two-Constant Equation of State. Ind. Eng. Chem. Fundam. 1976, 15, 59−64. (48) Cracknell, R. F.; Nicholson, D.; Quirke, N. A Grand Canonical Monte Carlo Study of Lennard-Jones Mixtures in Slit Shaped Pores. Mol. Phys. 1993, 80, 885−897. (49) Bloomer, O. T.; Gami, D. C.; Parent, J. D. Physical−Chemical Properties of Methane−Ethane Mixtures; Research Bulletin 22; Institute of Gas Technology, 1953. (50) Michalec, L.; Lisal, M. Molecular Simulation of Shale Gas Adsorption onto Overmature Type II Model Kerogen with Control Microporosity. Mol. Phys. 2017, 115, 1086−1103. (51) Bousige, C.; Ghimbeu, C. M.; Vix-Guterl, C.; Pomerantz, A. E.; Suleimenova, A.; Vaughan, G.; Garbarino, G.; Feygenson, M.; Wildgruber, C.; Ulm, F.; Pellenq, R. J.; Coasne, B. Realistic Molecular Model of Kerogen’s Nanostructure. Nat. Mater. 2016, 15, 576−582